

Sandia National Laboratories, California
Basic Energy Sciences - Materials Sciences Program

Selected Highlights FY1999

Prepared March 7, 2000

Science of Metals

In-Situ STM Studies of Thin-Film Dislocation Networks Under Applied Stress.....	2
Alloying at surfaces by the migration of reactive two-dimensional islands.....	4
Observation of Misfit Dislocation Glide on Surfaces.....	6
Spatial Order and the Evolution of Deformation – Induced Structures.....	8
Morphological Evolution of Grain Boundary Facets.....	10
The Role of Stress in Thin Film Alloys.....	12
Determination of Buried Dislocation Structures by Scanning Tunneling Microscopy	14
Failure of 1-D Models for Ir Island Diffusion on Ir(111).....	16
Aluminum Grain Boundary Sliding.....	18
Anomalous Exchange Interactions in III-V Dilute Magnetic Semiconductors.....	20
Effects of biaxial strain and chemical ordering on the band gap of InGaN.....	22

Alloy Theory

First-Principles Theory of Surface Alloys.....	24
Ab Initio Molecular Dynamics Simulations of Liquid Ni-Al Alloys.....	26
Thermodynamic Properties of Al-Cu Alloys.....	28
Thermodynamic Properties of Al-Sc Alloys.....	30

Advanced Ceramics

Imaging the Oxidation of the NiAl (110) Surface.....	32
Bulk Vacancies are Created at Surface Steps.....	34

In-Situ STM Studies of Thin-Film Dislocation Networks Under Applied Stress

O. Schaff, A.K. Schmid, N.C. Bartelt, J. de la Figuera and R.Q. Hwang

Motivation:

A great variety of different, well-ordered dislocation networks can be observed in different cases of heteroepitaxial metal thin films. The potential usefulness of these networks in the fabrication of nanostructured films with novel properties motivates the search for a fundamental understanding of them.

Accomplishment:

Generally, surface stress is invoked as the driving force for these dislocation networks. To test this conjecture, we compared predictions obtained from a detailed computer model with measurements obtained using a unique new instrument – the “stress-STM”. This device is capable of imaging a sample surface while the sample is strained by independently operated actuators. In this manner, the surface strain imposed by the lattice misfit of the film and substrate can be modified through the externally applied strain.

The herringbone-reconstruction on the Au(111) surface (Figure) is a prototypical example of a strain-driven dislocation network. For our experiments we used thin Au(111) gold crystals grown epitaxially on mica substrates. By elastically bending these structures, we were able to strain the gold crystals by up to 0.5%. We find that under uniaxially applied strain a dramatic restructuring of the network takes place. The three-fold orientational degeneracy of the system is removed and threading edge dislocations are annihilated.

The results are consistent with the idea that arrays of parallel Shockley partial dislocations (Figure) mainly relieve stress in a direction perpendicular to the dislocation lines. Parallel to the Shockley partials, the surface layer is still under high tensile stress. Partially relieving the tensile surface stress through the externally applied compression lowers the energy of stress domains. The dramatic dislocation rearrangements we observe in stressed samples are consistent with our calculations based on a 2D Frenkel-Kontorova model. In particular, the observed removal of the threading edge dislocations present in the unstressed herringbone reconstruction can be understood quantitatively: the energy difference between Shockley partial dislocations oriented parallel versus perpendicular to applied strain exceeding 0.1 % is far greater than the energy associated with the threading edge dislocations.

Significance:

We have shown how the characteristic dislocation networks present on the surfaces of Au thin films can be changed by bending the substrates to which the films are attached. Monitoring such changes as a function of strain in thin films offers a precise experimental probe of the balance between the various forces that are responsible for the complicated dislocation networks that often occur on metal surfaces.

Publications:

“In-Situ STM Studies of Strain-Stabilized Thin-Film Dislocation Networks Under Applied Stress”, Oliver Schaff, Andreas K. Schmid, Norm C. Bartelt, Juan de la Figuera and Robert Q. Hwang, accepted for publication in: *Materials Science and Engineering A* (2001)

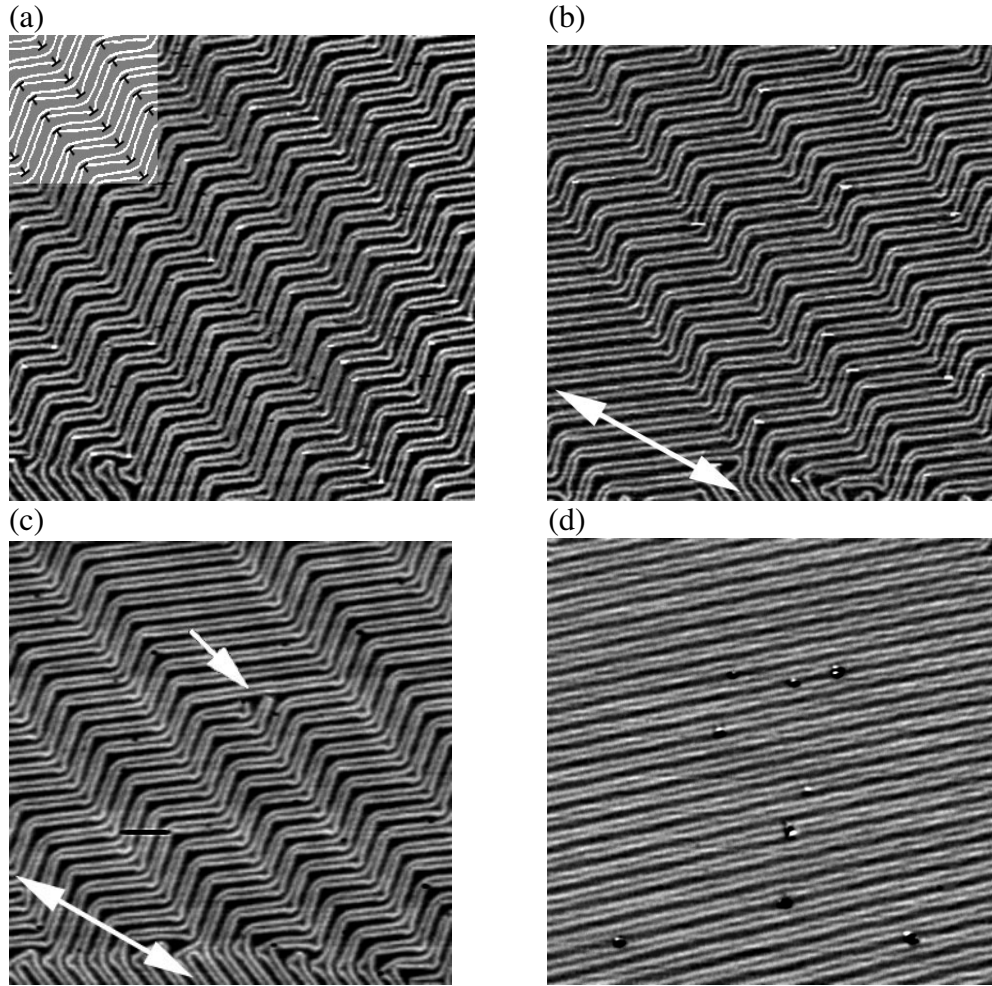


Figure: 170 X 170 nm² STM images of Au(111) under various conditions of applied stress. Doubleheaded arrows in (b) and (c) indicate the direction in which the mica substrate surface was compressed.

- 2) Well-annealed surface before application of external stress. The inset highlights the dislocation structure. Narrow domains of parallel Shockley partial dislocations (white lines) running along the [11-2] direction alternate with narrow domains of Shockley partials running along [-211]. Black symbols in the inset mark the positions of end-on perfect edge dislocations in the domain walls.
- 3) Uniaxial compressive stress of 0.17 % was applied. The same sample region as in (a) was imaged after briefly annealing above 80 °C. Relative coverage of one type of domain has increased by shifting domain walls.
- 4) Upon increasing the stress to 0.23 % and annealing again, the relative coverage of the dominant domain increases further through the elimination of minority domains, an example is indicated by an arrow.
- 5) Ultimately, the process often leads to the formation of large domains free of end-on edge dislocations. The image shows a different sample after annealing under 0.4 % uniaxial compression.

Alloying at surfaces by the migration of reactive two-dimensional islands

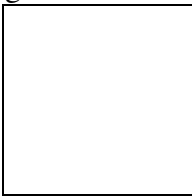
A.K. Schmid, N.C. Bartelt, and R.Q. Hwang

Motivation:

Several novel surface alloys have been discovered recently. The ability to control the nanoscale structure of these alloys offers a powerful opportunity to manipulate chemical and magnetic properties of surfaces. An understanding of the precise sequence of atomic events occurring during surface alloying is clearly desirable and does not exist at present.

Accomplishment:

To investigate the dynamic mechanisms of surface alloy formation, we have deposited Sn atoms on top of a Cu (111) surface at room temperature. As one would expect, after some time the Sn exchanges into the surface to form a surface bronze alloy. Surprisingly, however, we find that the dynamic process of this alloying is unexpectedly complex and occurs through a previously unknown mechanism involving the cooperative motion of clusters containing some 100,000 atoms. Using a combination of atomic resolution scanning tunneling microscopy (STM) and low-energy electron microscopy (LEEM) we find that shortly after Sn deposition large 2-D Sn islands coalesce on the Cu surface. These islands proceed to run across the surface. As they move, Sn atoms within the islands randomly exchange with Cu atoms in the surface. The exchanged Cu atoms are ejected from the Sn islands in the form of ordered 2-D bronze crystals

with a  structure. Sn islands consistently move away from their trail towards unalloyed regions of the Cu surface. We are able to trace the motion of the Sn islands to a simple atomic fact: Sn atoms on top of the Cu surface are strongly repelled by Sn atoms already incorporated into the Cu. The islands thus lower the free energy of the surface by moving. We find that island velocity is independent of size, consistent with a model in which the mobility of the Sn islands is determined by diffusion through the interior of the islands.

Significance:

The newly discovered mechanism of nanocluster motion, driven by surface free energy, should be a general mechanism of surface alloying when surface diffusion is faster than exchange into the substrate. Likely, other surface alloy systems will be found to exhibit similar dynamics.

Publications:

- 6) "Bronze Formation and the Motion of Mesoscopic Tin Clusters on a Copper Surface", Andreas K. Schmid, Norm C. Bartelt, and Robert Q. Hwang, *Surface Review and Letters* **7**, 515 (2000)
- 7) "Alloying at Surfaces by the Migration of Reactive Two-Dimensional Islands", A.K. Schmid, N.C. Bartelt, and R.Q. Hwang, *Science* **290**, 1561 (2000)

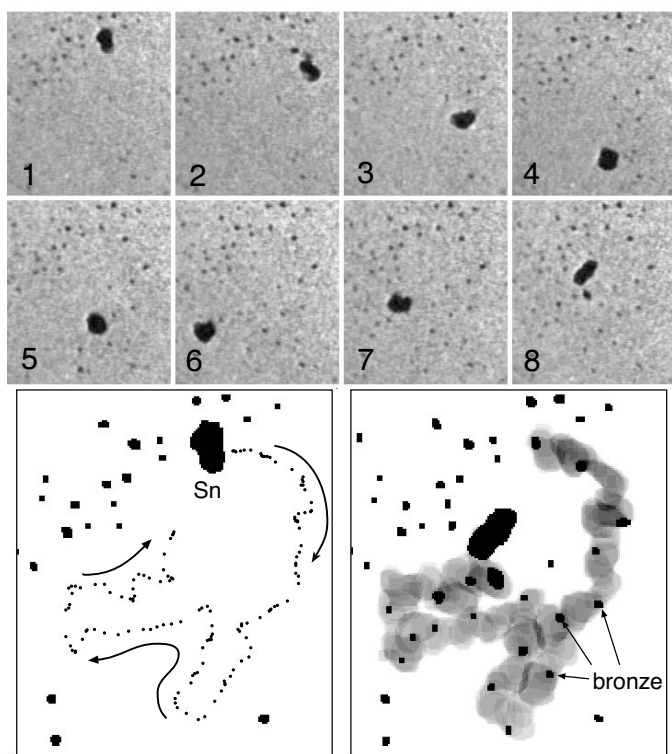


FIG. 1: Upper panels show a sequence of LEEM images (600nm wide) of a Sn island running on a Cu(111) surface at 290K. The time between images is 36 seconds. The large black object is the Sn island; the small static dark objects are ordered bronze islands that have been ejected from the Sn island. Lower left panel shows the trajectory of the center of mass of this island. The lower right panel shows the superposition of the intermediate positions of the islands: the gray level indicates how long the Sn island was over each position on the surface

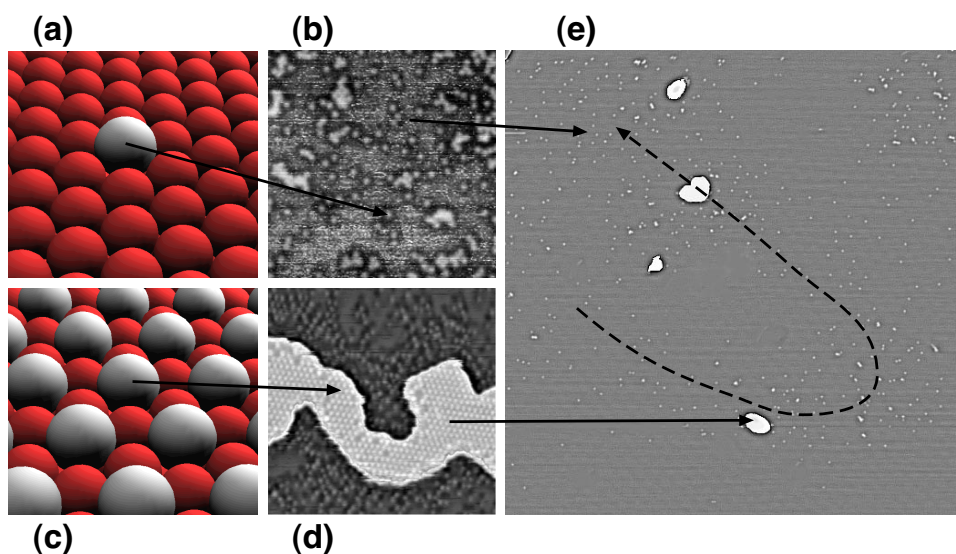


FIG. 2: ((a) and (c)) Schematic atomic configurations, and ((b) and (d)) atomic-resolution (15nmx15nm) STM images of bronze formation hours after Sn deposition on the Cu(111) surface. White spots in (b) are single Sn atoms embedded in top layer of Cu crystal, as suggested schematically in (a) where Cu atoms are red and Sn atom is white. (d) STM image

of structure of ordered atomic layer bronze islands as shown schematically in

Observation of Misfit Dislocation Glide on Surfaces

J. de la Figuera,, A. K. Schmid, N. C. Bartelt, and R. Q. Hwang

Motivation:

Misfit dislocations in thin metal films affect many of the physical properties of the surfaces, such as surface morphology, chemical reactivity, alloying properties and epitaxial growth. Understanding how these dislocations form and move is thus of fundamental importance. Unfortunately very little is known about dislocation motion at surfaces, especially compared to simple adatom diffusion. Part of the reason for this is that there are comparatively few cases where the atomic structure of the dislocations have been observed as the dislocations move.

Accomplishment:

We have observed thermally induced dislocation glide, and we have performed calculations by means of the Frenkel-Kontorova (F-K) model that help to understand the low energy barrier involved in the gliding process. The experiments have been done on single monolayer Cu films on Ru(0001) grown under Ultra-High-Vacuum conditions. The films present misfit dislocations of pure edge character with the Burgers vector in the plane of the film. Due to the presence of energetically comparable fcc and hcp adsorption sites, each misfit dislocation relaxes into two parallel Shockley partial dislocations bounding a stacking fault, and appears as two bright lines in Scanning Tunneling Microscopy images. Some dislocation segments have been imaged as a superposition of segments at different positions on the surface (see Figure 1). This multiple image effect is the result of the dislocations moving during the imaging process.

Whether the glide motion can occur easily depends on the size of the Peierls barrier to the motion. We compare our observations of the structure and the motion of the dislocations with results of the Frenkel-Kontorova model (where the input parameters were obtained from *ab-initio* calculations). The low barrier for glide is explained by the extended core structure of the threading dislocation (TD) that terminates each misfit dislocation. The extended core is due to the dissociation of the pure edge TD into a pair of partial Shockley threading dislocations. The calculated Peierls barriers are compatible with the experimental observations (see Figure 2). Additional measurements of the stiffness of the dislocations also agree with the predictions from the F-K model.

Significance:

The stiffness of the misfit dislocations has been measured. The structure of the threading dislocations which limit the glide process has been resolved. They are the analog of bulk jogs, where jog glide is believed to be an important component of bulk deformation processes. The predictive capability of the F-K model (when coupled to *ab-initio* calculations) has been validated. The observed dislocation motion is a surface self-diffusion mechanism that in principle could be competitive with adatom diffusion on close-packed surfaces.

Publications:

“Direct Observation of Misfit Dislocation Glide on Surfaces”, J. de la Figuera, K. Pohl, O. R. de la Fuente, A. K. Schmid, N. C. Bartelt, C. B. Carter and R. Q. Hwang, accepted for publication in Phys. Rev. Letters.

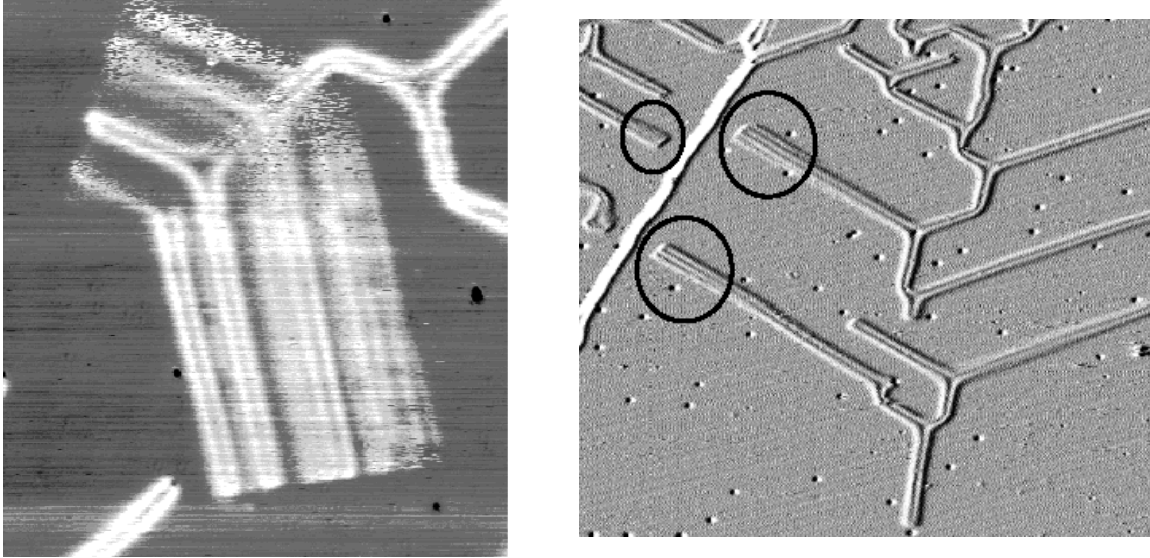


Figure 2. STM images of moving misfit dislocations. The moving dislocations appear superimposed due to the slow acquisition rate of the STM (minutes per image) relative to their movement. Left: Image size is 40nm. Several branches of a misfit dislocation are imaged superimposed. Right: Image size is 100nm. The circles mark misfit dislocations that appear blurred or superimposed.

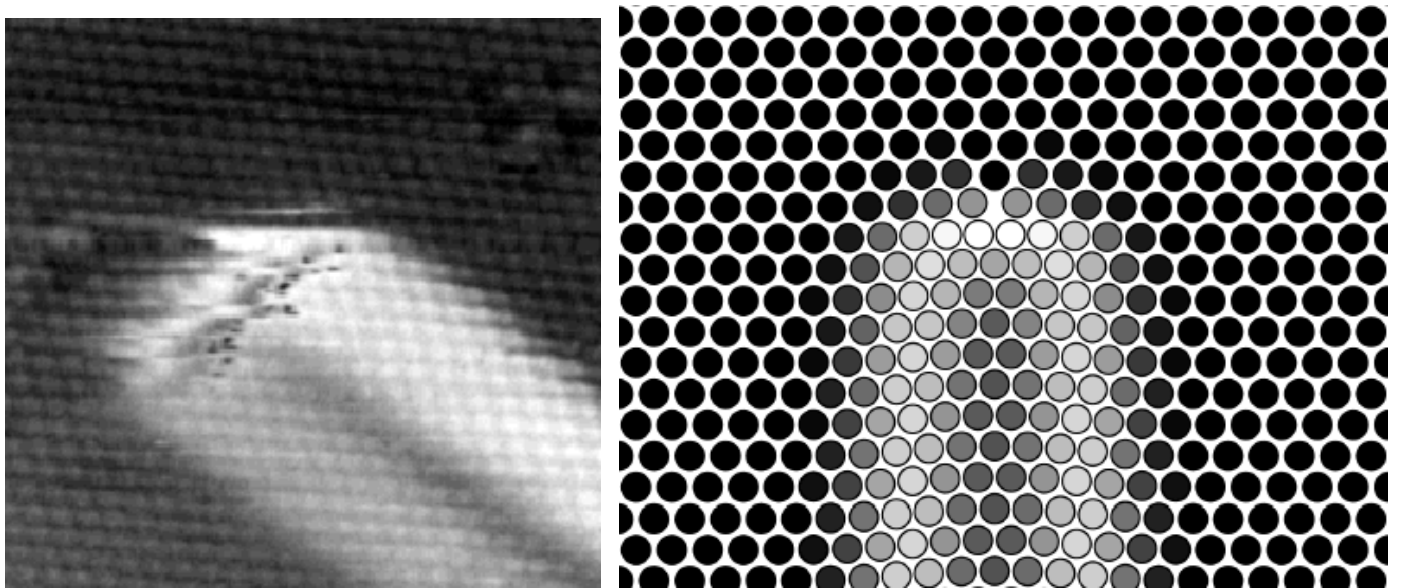


Figure 1. Left: experimental STM image (size 60nm) of the ending of a misfit dislocation. Right: Frenkel-Kontorova model of the same area.

Spatial Order and the Evolution of Deformation –Induced Structures

Darcy A. Hughes¹ and Maria C. Bartelt^{1,2}

¹SNL/CA , ²current address LLNL

Motivation:

Deformation of metals and alloys typically leads to a complex system of thin, dislocation-rich boundaries separating nearly dislocation-free regions (Fig. 1). This boundary arrangement determines material properties, with mechanical strength closely relating to the characteristic spacing between boundaries. A model for the evolution of the boundary spacing distribution with increasing strain would therefore provide a formalism to predict properties based on this evolution.

Accomplishments:

The arrangement of experimental boundaries reveals short-range order. Additionally, experimental observations show that boundary spacing distributions $P(D, \epsilon)$ at different strain levels collapse to a universal distribution when each distribution is scaled by its average spacing, D_{av} (Fig. 2a). We exploit these features and the strain invariance to develop a model of the evolution of the boundary spacing distribution. The goal is to predict locations and rates at which new boundaries are formed and old boundaries are removed. Consider that $P(D, \epsilon)$ evolves according to:

$$dP(D, \epsilon)/d\epsilon \approx \int_0^\infty dy P(y, \epsilon) r_{CR}(y-D, D, \epsilon) - P(D, \epsilon) \int_0^D dy r_{CR}(D-y, y, \epsilon), \quad (1)$$

with $P(D, 0)=0$, where $r_{CR}(y_1, y_2, \epsilon)$ describes the odds of creating a boundary which splits the spacing y_1+y_2 , between two adjacent boundaries, into two new spacings, y_1 and y_2 . If one chooses the simplest function $r_{CR}(y_1, y_2, \epsilon)=(y_1+y_2)^\alpha$, that is not dependent on strain, then integration of equation 1 yields the approximate analytical expression:

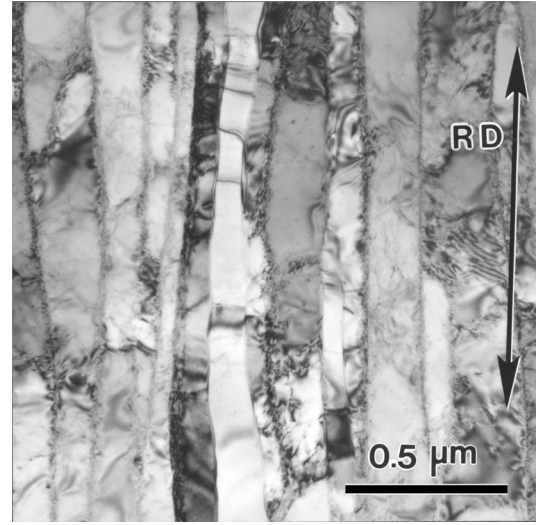
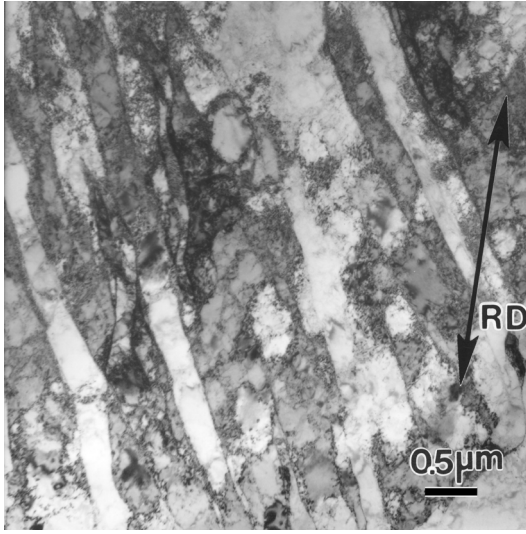
$$P(\zeta, \omega) \approx c\omega \zeta^{\alpha+1} \exp(-\omega \zeta^{\alpha+1}), \quad (2)$$

with $c=(1/D_{av})(1+\alpha)^2 \omega^{1/(\alpha+1)}/\Gamma[1/(\alpha+1)]$, $\zeta=D/D_{av}$, and $\omega=\epsilon D_{av}^{\alpha+1}$. Equation 2 is only independent of the strain if $\omega=\epsilon D_{av}^{\alpha+1}$ is a constant. This constraint is checked in Fig. 2b showing that this strain dependence of D_{av} is observed. The strain dependence also suggests a value of α which is 1/2. This choice of α weights the creation of a new boundary between adjacent boundaries by the square root of the spacing thereby providing an excellent fit of the scaling function to the experimental data, Fig. 2a.

Significance:

The success of this statistical model in describing the results, despite the complexity of boundary formation, provides us with a new and rational means to construct models of microstructure. Such models provide a basis for discussion of how mechanical properties can be engineered efficiently within the many high volume industries associated with the deformation processing of metals and alloys.

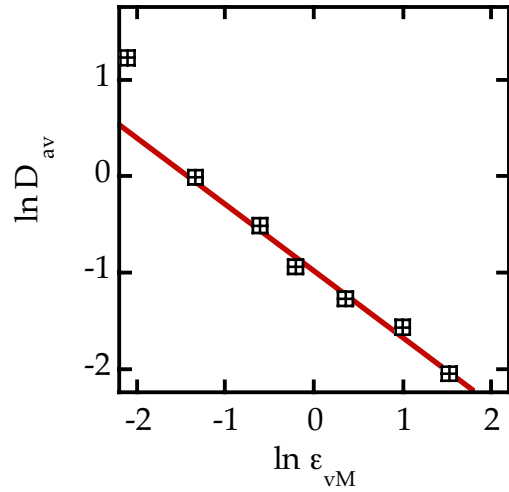
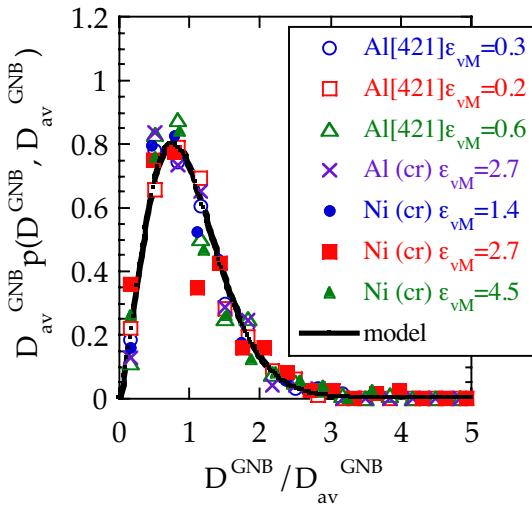
M. C. Bartelt and D. A. Hughes, “Spatial Order and the Evolution of Deformation-Induced Structures,” submitted for publication, 2001.



a)

b)

Figure 1. Extended dislocation boundaries following different amounts of cold rolling nickel look similar when the magnification is scaled by the average spacing, D_{av} . a) following 37% cold reduction, b) following 95% cold reduction



a)

b)

Figure 2. a) Universal distributions for cold rolled nickel and compressed aluminum single crystals showing the model fit, eqn.2, based on $\alpha=1/2$ derived from the experimental data in b) for nickel, b) Strain dependence of D_{av} for cold rolled nickel showing a power law relation.

Morphological Evolution of Grain Boundary Facets

D.L. Medlin and G. Lucadamo

Motivation:

Grain boundaries are often faceted in extreme cases of interfacial anisotropy. Such a morphology prevents the application of classical notions of grain-boundary curvature to understanding microstructural evolution. Although there has been much effort at incorporating anisotropic grain-boundary properties, including faceted geometries, into computational approaches for microstructural evolution, at present our mechanistic understanding of the behavior of facets and their junctions remains limited.

Accomplishment:

We are conducting experiments to better understand the behavior of facets during grain evolution. Our initial focus is on the dynamics of $\Sigma=3$ $\{11\bar{2}\}$ facets in $\langle 111 \rangle$ oriented gold thin films. This system is well suited for these studies since the crystallography and structure of the boundaries is already well understood. An example of one such faceted grain is shown in Figure 1a to illustrate the fine-scale facet distribution typical of the initial, as-deposited films. As shown in Figure 1b, annealing dramatically increases the fraction of the boundary length composed of larger-scale facets. In order to determine the pathway by which this coarsening occurs, we are using *in situ* transmission electron microscopy to track the real-time evolution of the boundaries. The transition from an initial highly stepped boundary to a single corner is shown in the series of micrographs in Figure 2. From these observations, we have learned that the grain boundary facet coarsening is accompanied by the motion of perimeter conserving facets (*i.e.*, facets terminated by corners of opposite sense with respect to the Wulff surface).

Significance:

Our observations are surprising in light of the conventional view of grain-boundary facet evolution. Perimeter conserving facets have been thought to remain fixed until being passively consumed by facets terminated by corners of the same sense (which do not conserve the boundary perimeter and thus lead to a net reduction in interfacial energy). However, no explicit properties are assigned to the corners in such phenomenological constructions--junctions are treated simply as the geometric consequence of joining two facets. Thus an important question is raised: are there energetics associated with the junctions themselves that produce a driving force for facet motion? To address this question, we are currently measuring the short-time fluctuations in junction position to determine whether correlations exist that would be indicative of junction-junction interactions.

Publication:

"Morphological Evolution of a Fully Faceted Grain Boundary," D.L. Medlin and G. Lucadamo, in "Influences of Interface and Dislocation Behavior on Microstructure Evolution," eds. M. Aindow *et al.* (2001, MRS) (in press).

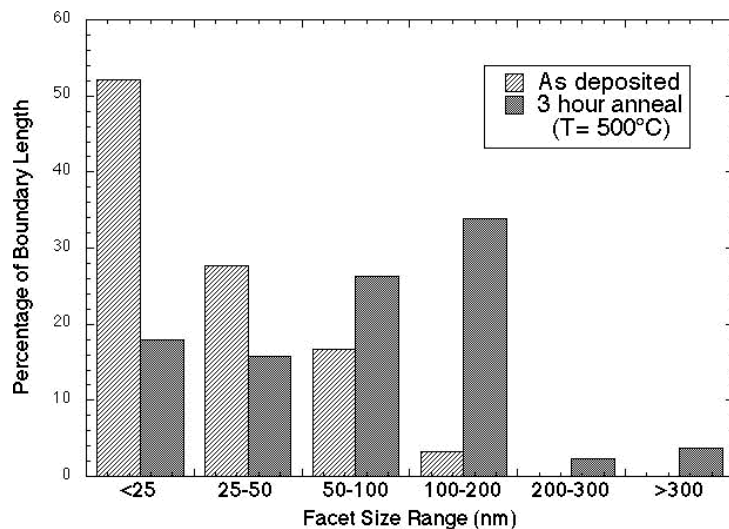
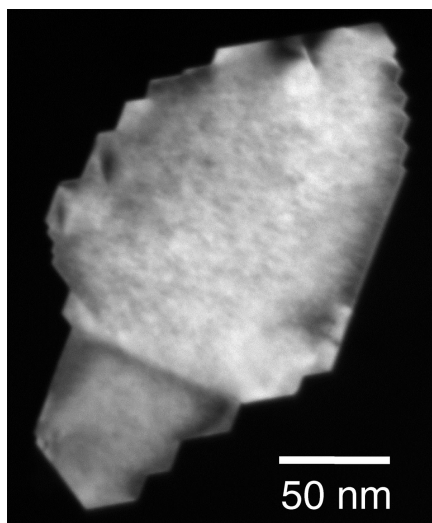


Figure 1. (a) Darkfield micrograph showing facet steps on an enclosed grain in an as-deposited $\Sigma=3$ Au film. (b) Graph shows the proportion of total grain-boundary length as distributed across the range of facet sizes for grains before and after annealing. Prior to annealing, the majority of facets are smaller than 50 nm. With annealing, an increased proportion of boundary length shifts to larger facet size.

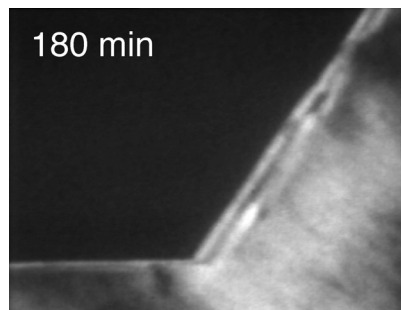
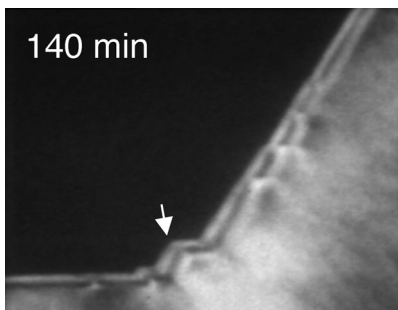
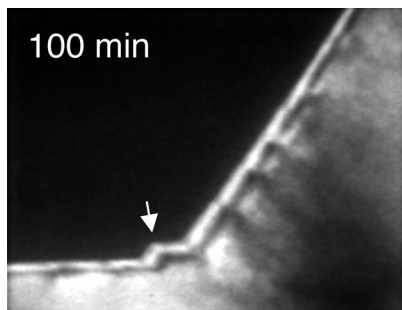
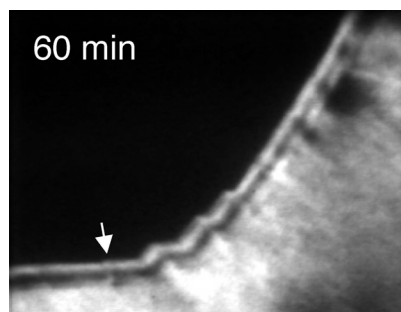
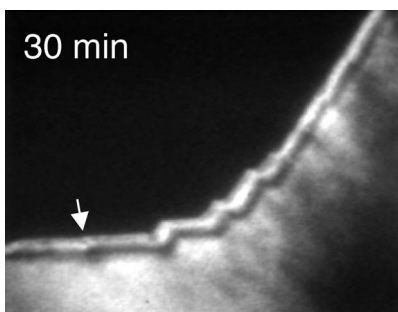
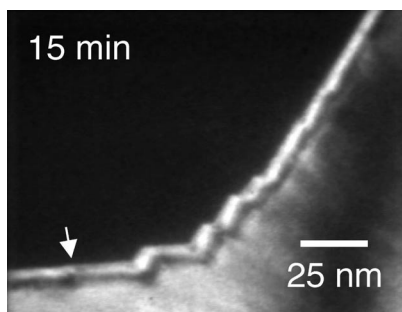


Figure 2. Stills taken from video showing motion of facets during evolution of boundary corner during annealing ($T=490^{\circ}\text{C}$). The arrowed feature tracks a junction pair as it grows from a barely detectable feature in the initial stages to a well defined step (100 and 140 minutes) before shrinking again as the final corner develops.

The Role of Stress in Thin Film Alloys

G.E. Thayer, V. Ozolins, A.K. Schmid, N.C. Bartelt, R.Q. Hwang

Motivation:

Surface stress due to crystalline lattice mismatch is well known to have a profound influence on the structure of surfaces and interfaces. Because interfacial structure is a dominant factor in the determination of new and interesting properties found in thin film structures and multilayer superstructures, a detailed understanding of the relation between surface stress and surface structure is important. Such an understanding requires an investigation in which theory and experiment are closely coupled.

Accomplishment:

We have investigated surface stress by using experimental measurements to make a detailed thermodynamic phase diagram of the structure of a surface alloy and comparing it to well defined theoretical models. This study took advantage of the abilities of scanning tunneling microscopy (STM) to image surfaces with atomic resolution to observe the structure of submonolayer CoAg films on Ru(0001). CoAg/Ru(0001) consists of two immiscible metals, Co and Ag, each with oppositely induced surface stress when deposited on Ru (due to lattice mismatch), which causes a thin film alloy to form. Comparing the measured phase diagram with first-principles local-spin-density-approximation (LSDA) calculations, we discovered that multiple stress relief mechanisms resulted in a surface phase diagram that is different from the relatively simple progression of droplet and stripe phases predicted by well accepted continuum theories. The experimental data revealed a phase separation that the theory had not predicted. Figure 1a shows a submonolayer $\text{Co}_{0.8}\text{Ag}_{0.2}$ alloy film extending from a Ru step edge. When a different film with a higher concentration of Ag was imaged, the film was found to consist of two phases, a $\text{Co}_{0.6}\text{Ag}_{0.4}$ alloy phase and a pure dislocated Ag phase (Figure 1b). This observation led to the improvement of our theoretical model that was then able to more closely match the experimental results. In structural investigations on a more local scale (10\AA), measured displacements of highly strained Co atoms found at the boundaries between Ag and Co (Figure 2) were compared to calculated data and found good agreement. This work was able to verify models that include short-range chemical forces and long-range elastic or electrostatic forces within an order of magnitude.

Significance:

Using a combined experimental and theoretical approach, our investigation of CoAg/Ru(0001) has contributed to a more detailed understanding of the relation of surface stress to surface structure. The agreement between theory and experiment in this complicated system confirms the accuracy of our models and our ability to predict which interactions are involved on surfaces and their magnitudes. Since similar long-range and short-range interactions as well as stress relief mechanisms will be features common to many surfaces and interfaces, these results in part contribute to understanding the factors that control the formation of new thin-film materials.

Publications:

1. G.E. Thayer, V. Ozolins, A.K. Schmid, N.C. Bartelt, M. Asta, J.J. Hoyt, S. Chiang, and R.Q. Hwang, "Role of Stress in Thin Film Alloy Thermodynamics: Competition between Alloying and Dislocation Formation", *Physical Review Letters*, 2001. **86**(4): p. 660-663.

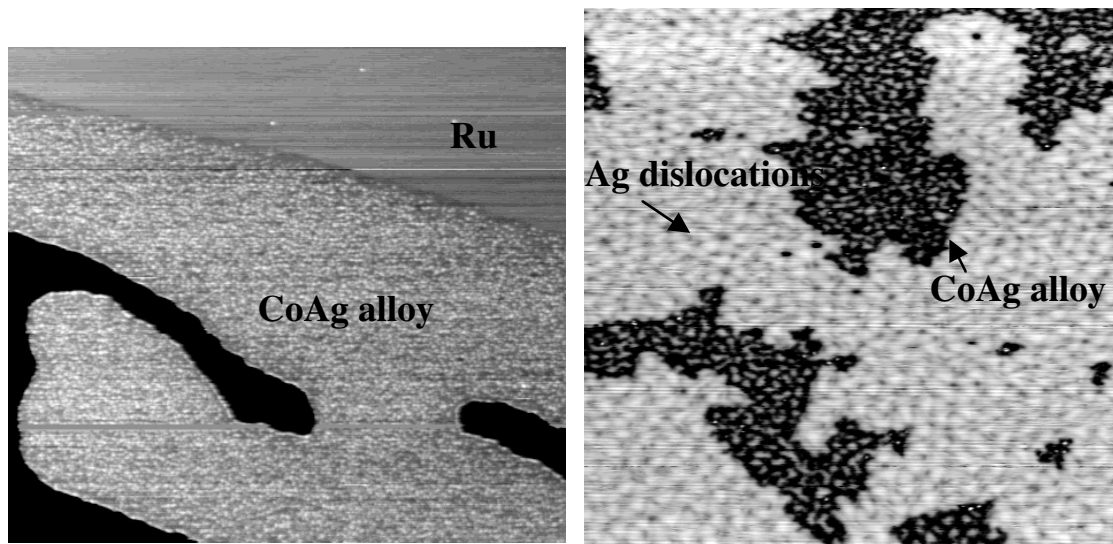


Figure 1(a) Equilibrated CoAg films on Ru(0001). Phase segregation occurs for films with Ag composition greater than 40%. (a) $1890\text{\AA} \times 1680\text{\AA}$ image ($I_t = 0.24\text{ nA}$, $V_s = -0.16\text{ V}$) of submonolayer alloy film with composition of 25% Ag shown against two Ru terraces in the background.

Figure 1(b) $1000\text{\AA} \times 1000\text{\AA}$ image ($I_t = 0.50\text{ nA}$, $V_s = 0.58\text{ V}$) of film with composition of 80% Ag. Inset shows atomic resolution of a single dislocation in the pure Ag phase, showing that a row of atoms goes missing in the atomic lattice.

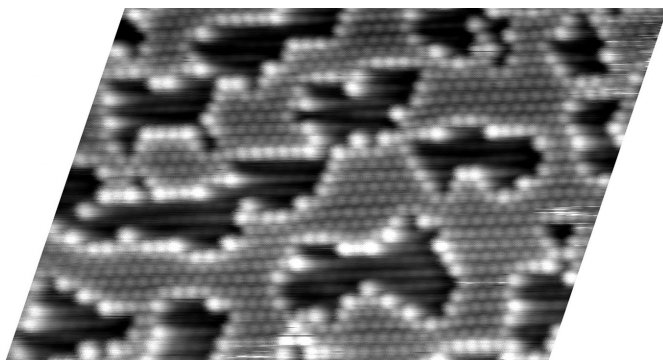


Figure 2 Atomically resolved image of CoAg thin film alloy. Highly strained Co atoms at borders of Co and Ag regions are indicators of surface stress due to lattice mismatch.

Determination of Buried Dislocation Structures by Scanning Tunneling Microscopy

J. de la Figuera, A. K. Schmid, N. C. Bartelt, and R. Q. Hwang

Motivation:

Misfit dislocations in thin metal films affect many of the physical properties of the surfaces, such as surface morphology, chemical reactivity, alloying properties and epitaxial growth. Determining their detailed structure continues to represent a challenging problem to experimentalists. For bulk samples, full characterization of dislocation networks at phase boundaries is sometimes possible through the examination of cross-sectional samples in transmission electron microscopy (TEM). However, determining the structure of dislocations that are parallel to the interface is difficult.

Accomplishment:

We demonstrate that for close-packed fcc or hcp systems detailed information on the nature of buried dislocations can be extracted from controlled Scanning Tunneling Microscope (STM) experiments. In particular we are able to determine the atomic plane in which thin-film dislocations reside through a careful geometrical analysis.

To identify the stacking sequence of Cu films on Ru(0001) we have examined films with incomplete layers. The structure of films with thickness between 1 and 3 ML have been determined by a step-by-step comparison of how unknown parts of a film match with regions of known stacking sequence. The 1ML case is described in the top figure.

The result from the analysis is the presence of several competing stacking sequences for each film thickness. Shockley partial dislocations at the Cu-Ru interface separate the different stacking sequences, although some dislocations located at higher levels can also be found. The dislocations located at higher layers can be interpreted as twin boundaries (see bottom figure). For thicker films, all the stacking sequences correspond to fcc Cu.

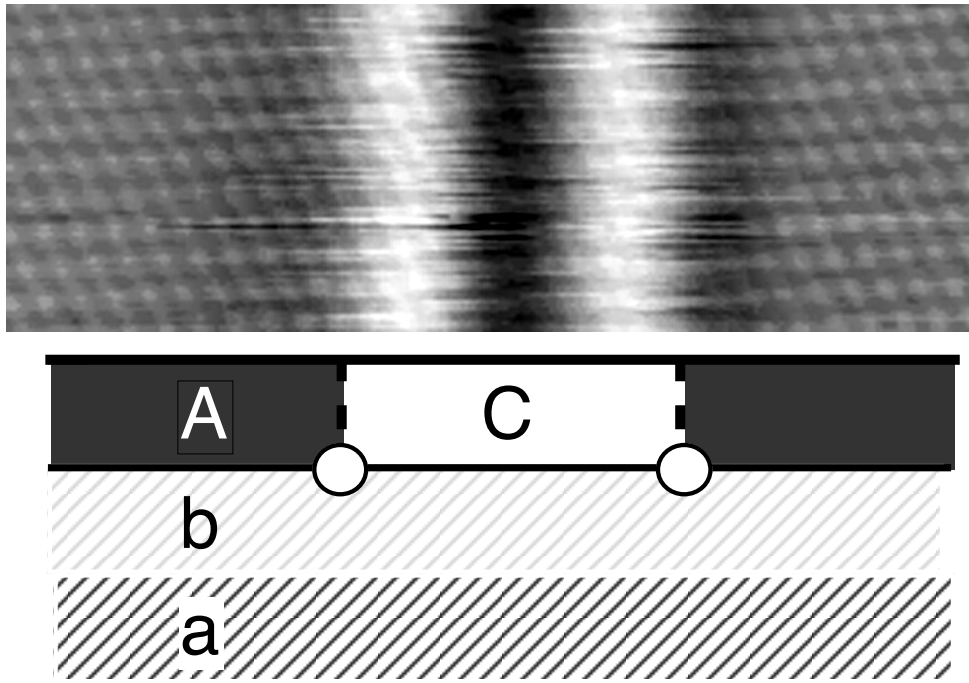
In the particular case of 2ML Cu on Ru, we have performed *ab-initio* calculations for the energies of the different stacking sequences possible. They agree with the experimental order of the energies of the stacking sequences, as obtained through a comparison of the width of the different regions as seen by STM.

Significance:

The misfit dislocation networks of Cu on Ru(0001) have been presented as a model system of stress relief in metal thin films. But up to this work, the detailed characterization by a local probe of the position of the dislocation networks observed in the film was lacking. The method, being purely geometrical, should be applicable to other misfit dislocation patterns in thin metal films grown on hexagonal substrates.

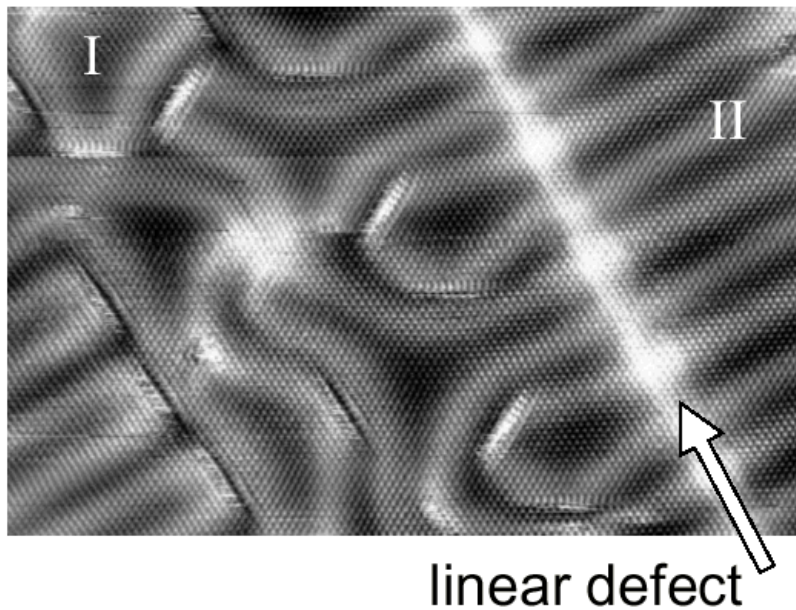
Publications:

“Determination of Buried Dislocation Structures by Scanning Tunneling ”, J. de la Figuera, A. K. Schmid, N. C. Bartelt, K. Pohl, and R. Q. Hwang, accepted for publication in Phys. Rev. B.



Top: STM image of a 1ML Cu film on Ru(0001), showing a misfit dislocation with atomic resolution. The sketch of the stacking sequence is shown below.

Bottom: STM image (40nm x 27nm) of a 3ML film of Cu on Ru(0001). Several dislocations are shown. The linear defect indicated by a white arrow is composed of two Shockley partials on successive Cu layers forming the start of a twin boundary between regions I and II.



Failure of 1-D Models for Ir Island Diffusion on Ir(111)

J. C. Hamilton and A. F. Voter

Motivation:

Field ion microscopy experiments have shown that 7 and 19 atom Ir clusters on Ir(111) have remarkably high prefactors for diffusion, more than 10^3 times greater than for single atom Ir diffusion on this surface. This observation has stimulated a number of different theoretical explanations, including a simple 1-D model (S.Y. Krylov, Phys. Rev. Lett. **83**, p. 4602) which claims to model the phenomena. The purpose of the investigation reported here was to calculate the diffusion prefactors in this simple model using classical trajectory methods and harmonic transition state theory. Since similar models have also been proposed to calculate molecular separation by zeolites, it is important to understand the diffusion rates predicted by such a model and to determine whether it exhibits high diffusion prefactors.

Accomplishment:

We investigated the properties of a 7-atom chain diffusing in a one-dimensional sinusoidal potential. The potential parameters were chosen to match the model proposed by Krylov. We used classical trajectory methods (molecular dynamics) and harmonic transition state theory (the Vineyard approximation) to determine the diffusion rates for this chain. Calculations of the transition states showed that this chain stretches or compresses so that the atoms pass sequentially over the sinusoidal potential barriers during diffusion (see figure 1). This is similar to a light wall or heavy wall dislocation mechanism for diffusion. The molecular dynamics results were in excellent quantitative agreement with the harmonic transition state theory. These results show that the prefactor for diffusion in this model is similar to the prefactor for diffusion of a single atom. We conclude that this model cannot explain the experimental observations for Ir clusters diffusing on Ir(111).

Significance:

We have calculated the activation energies and prefactors for diffusion of a 7-atom chain in a sinusoidal potential. We show that this simple model cannot account for the high prefactors observed in the diffusion of compact hexagonal Iridium islands on the Iridium (111) surface. This indicates that higher dimensional models and/or more realistic energy calculations will be required to explain the experimental observations.

Publications:

Failure of 1D models for Ir island diffusion on Ir(111), J. C. Hamilton and Arthur F. Voter, Phys. Rev. Lett., **85**, p. 1580, Aug. 14, 2000.

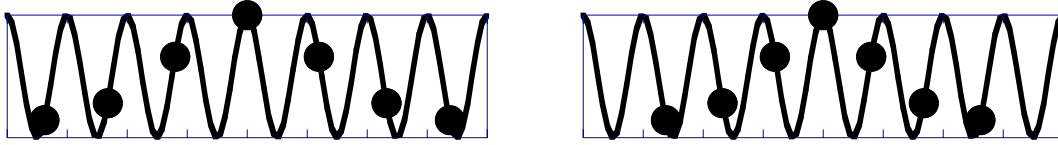


FIGURE 1: Transition states for seven atom chain in sinusoidal potential. The activation barrier for diffusion is lowered by stretching or compressing the chain as shown. This is a dislocation mechanism for diffusion, but our investigations show that the prefactor is similar to the prefactor for single atom diffusion

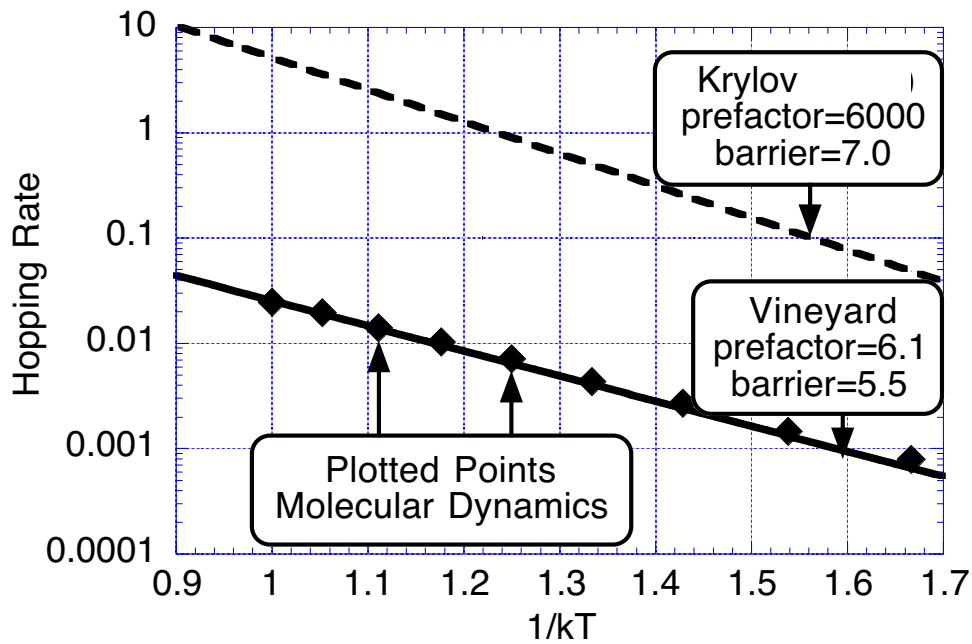


FIGURE 2: Arrhenius plot for diffusion rate of 7 atom chain in sinusoidal potential. The lower line shows the agreement between molecular dynamics and harmonic transition state theory (the Vineyard approximation). We do not see the dramatic prefactor enhancement predicted by Krylov, indicating that the Ir island on Ir(111) system cannot be described by this model.

Aluminum Grain Boundary Sliding

J. C. Hamilton

Motivation:

In the past we have pursued extensive experimental and theoretical investigations of grain boundaries. These studies have resulted in a detailed understanding of the static structure of aluminum grain boundaries. We are now extending our theoretical studies to include dynamic processes at grain boundaries, including grain boundary sliding. Grain boundary sliding is a complex process which dominates the deformation of polycrystalline metal samples at high temperatures (greater than 4/10 of the melting point).

Accomplishment:

We have used first principles nudged elastic band calculations to calculate the theoretical shear stress of the Aluminum $\Sigma 3$ $[11\bar{2}]$ incoherent twin boundary. This is a commonly occurring low energy grain boundary. It has two different stable configurations as shown in figures 1a and 1c. The stable configurations both have the $\{111\}$ planes on one side of the grain boundary offset by about 0.7\AA relative to the planes on the other side of the grain boundary. Figure 1b shows a symmetric configuration which is the intermediate in shearing from a to c. Further shearing from configuration c eventually produces the stable configuration shown in Figure 1e. This configuration is equivalent to configuration a.

Figure 1d shows an antisymmetric configuration which is the intermediate in shearing from c to e. The energy barrier associated with this shear is quite small, only about 10% of the energy required to shear bulk Aluminum along the facile $\{111\}$ shear planes.

Significance:

This calculation provides fundamental insight into the process of grain boundary shear. We find that the theoretical shear strength of this grain boundary is ten times smaller than the theoretical shear strength of bulk aluminum along the favored slip directions. This accounts for the major role which grain boundary diffusion can play in deformation of polycrystalline samples. We also note that the grain boundary translates in a direction perpendicular to itself as it undergoes shear. This phenomena has been seen experimentally in Zinc tilt boundaries. Our calculations demonstrate the precise atomic mechanism of this grain boundary translation during shear. We anticipate that the first principles results provided here will be useful in quantitative modeling of the structure of grain boundary partial dislocations at this grain boundary.

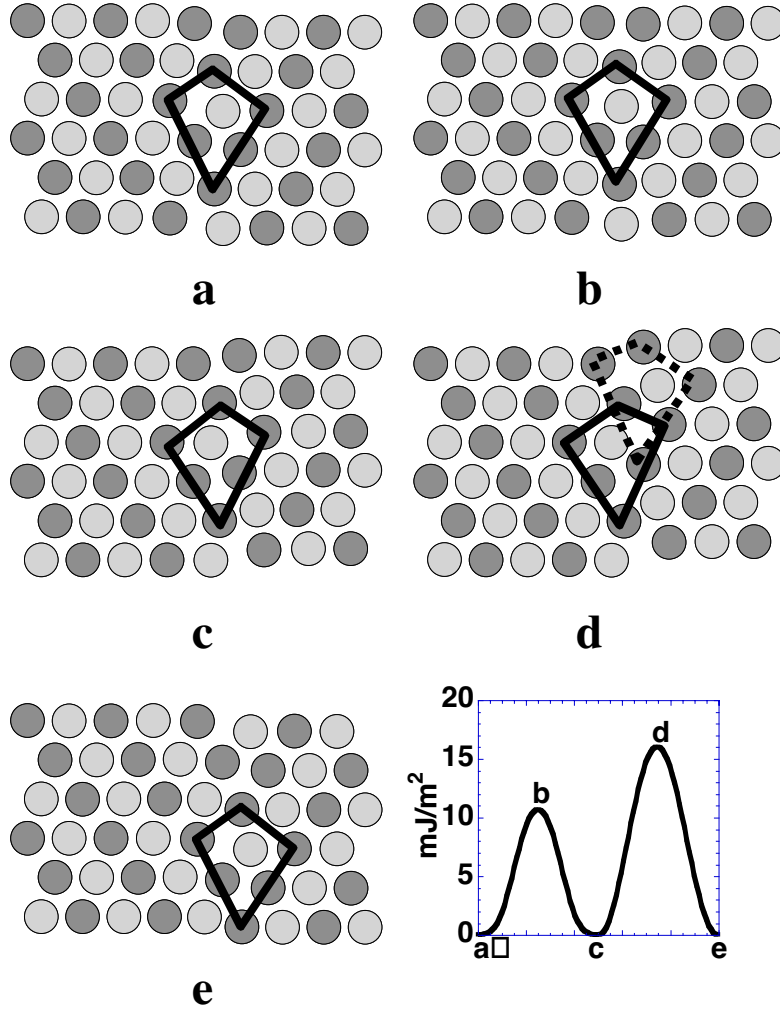


FIGURE 1: Structure and energy of Al $\Sigma 3$ $[11\bar{2}]$ grain boundary during shear. In (a), a stable configuration of the grain boundary is shown. The lattice on the right hand side of the boundary is offset downward by about 0.7 Å relative to the lattice on the left hand side of the boundary. In (b) the lattice on the right hand side of the grain boundary is displaced upward to match the lattice on the left hand side of the grain boundary. We call this the symmetric configuration. In (c) the lattice on the right hand side of the grain boundary is displaced further upward to reach a stable configuration which is related by a symmetry operation to the starting configuration in (a). In (d) the lattice on the right hand side of the grain boundary is displaced upward to reach a configuration with the right hand lattice planes half-way between the left hand lattice planes. We call this the anti-symmetric configuration. In (e) the right hand lattice has been displaced upward again and is now in a stable configuration with the same offset shown in (a). The grain boundary has moved to the right as a result of the sliding. The energy of these configurations determined by a nudged elastic band calculation is shown in the final graph.

Anomalous Exchange Interactions in III-V Dilute Magnetic Semiconductors

Mark van Schilfgaarde and O. N. Mryasov

Motivation

To explain magnetic interactions in Mn doped III-V Dilute Magnetic Semiconductors

Accomplishment

In recent years, metallic magnetic superlattices have enjoyed considerable success. They are now used commercially in magnetic read heads, and there is great interest in using them or magnetic superlattices with nonmagnetic spacers as electronic devices. Recently it was shown that the $\text{Mn}_x\text{Ga}_{1-x}\text{As}$ alloy, for $x < 0.10$, undergoes a spontaneous transition to a ferromagnetic state at temperatures to 100K. We studied the exchange interactions between magnetic dopants Cr, Mn, and Fe in the III-V compounds GaAs, GaN and AlN, using the local spin-density approximation. This work produced two independent findings, both of significance for these new, ferromagnetic III-V semiconductor alloys.

By considering small clusters and random configurations of magnetic dopants in GaAs and GaN, in the range of 1 to 5% concentrations, we model the exchange interactions. This is done by performing total-energy calculations of magnetic clusters in different spin configurations, and using the energy differences to map the magnetic energy into a model heisenberg hamiltonian. We show that the exchange interactions are anomalous and behave quite differently from the generally expected behavior, as predicted by the RKKY theory, or the celebrated Anderson superexchange model.

Fig 1 shows the calculated position of the d defect level in the host gap for an isolated transition-metal impurity. The position in the gap depends in a systematic way on the atomic number of the impurity. The Table shows the calculated Heisenberg pairwise interactions for nearest-, second- and fourth- neighbors deduced for a variety of clusters. It is seen that these interactions are strongly environment-dependent *and decrease with increasing dopant concentration*. Both effects are contrary to RKKY theory, and may explain the observed maximum in critical temperature with impurity concentration

Additionally the magnetism is responsible for a strong, short-range attraction between the magnetic dopants, thus creating an anomalous effective alloy hamiltonian. This suggests that the impurities may aggregate into small nanoclusters of a few magnetic atoms. Fig. 2 shows the heat of reaction by the splitting of two n -atom Mn clusters into an $n-1$ atom and an $n+1$ atom cluster. For small clusters, the energy is strongly negative, showing the tendency of the Mn to combine into small nanoclusters.

Significance

This work is the one of the first *ab initio* description of exchange interactions in these new materials, and are critical for elucidating a fundamental exchange interactions.

A paper has been submitted to Physical Review Letters.

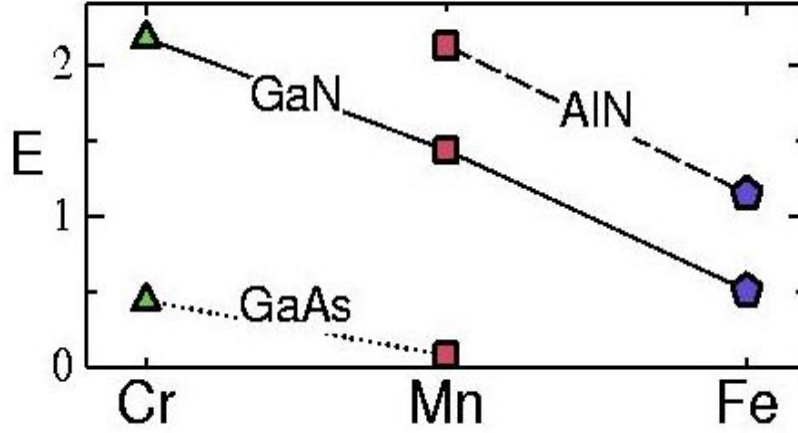


Fig. 1. Position of transition-metal d defect level in host semiconducting gap

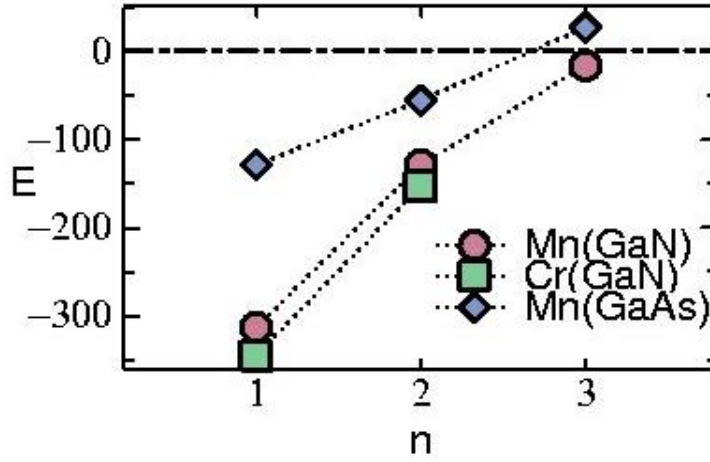









Fig. 2. Heat of reaction for 2 n -atom clusters to decompose into an $n-1$ atom cluster and an $n+1$ atom cluster, in meV.

Heisenberg parameters J_n (in meV) deduced from a Connolly-Williams prescription for various molecular clusters embedded in a 216-atom Σ B host. Symbols $[[$, $[[[$, $[[[[$, and $[[[[[$ refer to clusters of 2, 3, 4 (tetrahedron) and 5 (pyramid) magnetic atoms. J_n refers to the Heisenberg interaction between n^{th} nearest neighbors.

	$[[$ 	$[[[$ 	$[[[[$ 	$[[[[[$ 	$[[[2]$ 	$[[[3]$ 	$[[[4]$ 
	J_1	J_1	J_1	J_1 J'_1 J_2	J_2	J_1 J_2	J_2 J_4
Mn:GaAs	55	-41	24	14 30 -27	15	50 -11	9 20
Mn:GaN	78	-45	20	-2 13 -54	23	47 -15	9
Mn:AlN	51	10					
Cr:GaAs	89	52					

Effects of biaxial strain and chemical ordering on the band gap of InGaN

Mark van Schilfgaarde

Motivation

To understand the origin of bandgap bowing in InGaN semiconductor alloys.

Accomplishment

Wurtzite $\text{In}_x\text{Ga}_{1-x}\text{N}$ has a direct band gap that can be varied from 3.42 ($x = 0$) to 1.89 eV ($x = 1$) making it useful for fabricating blue and green light-emitting diodes. Recent experimental studies have begun to provide valuable insights into the properties of InGaN. In particular a (Stokes) shift is often seen between the peak in photoluminescence or electroluminescence spectra and the absorption edge typically used to define the band gap. Both composition fluctuations and the Franz-Keldysh effect reduce the bandgap, and these are generally attributed to the observed shifts. However, we show that there are two important contributions to the bandgap bowing in InGaN alloys not hitherto considered.

Another now well established experimental fact is that these alloys can accommodate unusually large strains under epitaxial growth. InGaN layers up to 2500 Å thick can remain coherent when grown on thick ($\approx 2\mu$) GaN films. Using the local density approximation, we show that strains of this magnitude are responsible for nonlinear corrections to the deformation potential, that tend to widen the gap for $x < 0.25$ and reduce the gap for $x > 0.25$.

Also, we show that chemical ordering of the In and Ga significantly reduces the gap relative to the random alloy. For wurtzite (WZ) crystals grown along the [0001] axis, there is a strong driving force for the In and Ga to order in alternating planes at the free surface, which if frozen into the bulk, generates the short-range order that is responsible for this ordering. This driving force does not exist for the ZB case, and thus can account for the observed difference in bowing between ZB and WZ crystals.

Fig. 1 shows experimental data for both ZB grown and WZ grown materials. It is seen that the bowing in the WZ case is significantly larger. Fig. 2 compares experimental ZB gaps (open symbols) to calculated values (filled symbols). In the latter, both ZB and WZ data are calculated for unstrained, random alloys, and the bowing is seen to be similar for the two cases. This shows that observed differences between ZB and WZ are probably connected to differences in growth conditions. Fig. 3 shows the effect of strain and cation ordering on the bowing. Both significantly alter the bowing, and apparently both are needed to account for the bowing observed in the WZ case, and explain the observed difference between WZ and ZB alloys.

Significance

These effects offer a simple and natural explanation for the observed bowing in WZ and ZB InGaN alloys, a technologically important alloy for blue lasers and diodes.

Reference

A. F. Wright, K. Leung, and M. van Schilfgaarde, Appl. Phys. Lett. **78**, 189 (2001).

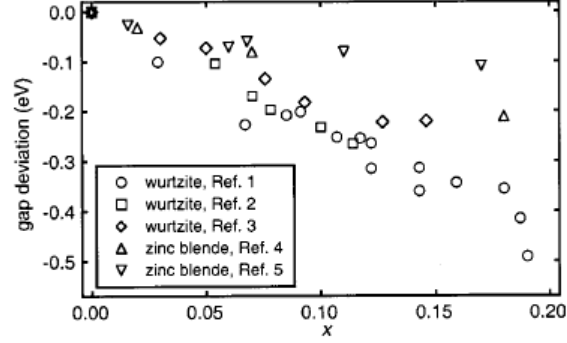


FIG. 1. Measured gap deviations for strained wurtzite and unstrained zinc-blende InGaN. The gap deviations are computed using measured band gaps for unstrained wurtzite and zinc-blende GaN from the corresponding references, and assuming band gaps of 1.89 eV for wurtzite InN and 1.80 eV for zinc-blende InN.

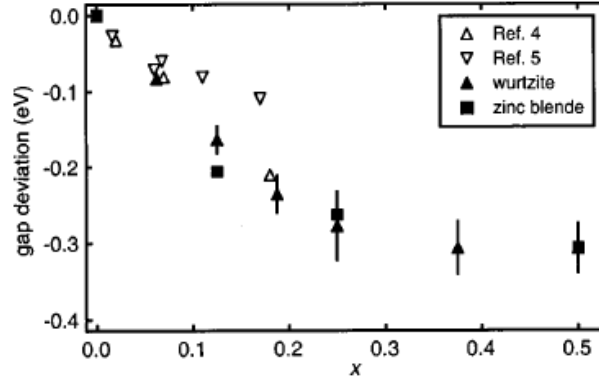


FIG. 2. Calculated gap deviations for random unstrained wurtzite InGaN, estimated gap deviations for zinc-blende InGaN, and corresponding experimental results for zinc-blende InGaN. The symbols for the wurtzite results show the average of the gaps from the five configurations and the vertical lines give the standard deviations.

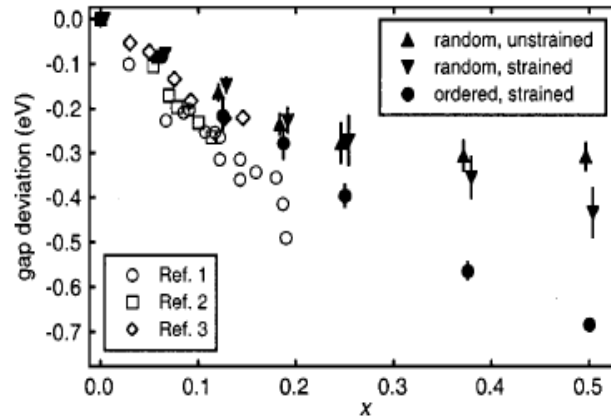


FIG. 3. Calculated and experimental gap deviations for wurtzite. The symbols for the wurtzite results show the average of the gaps from the five configurations and the vertical lines give the standard deviations. Note that we have offset the compositions for the random results by ± 0.003 to make them easier to distinguish.

First-Principles Theory of Surface Alloys

V. Ozolins,* N. C. Bartelt,* M. Asta,** and J. J. Hoyt***

**Sandia National Laboratories, Livermore, California*

***Department of Materials Science and Engineering, Northwestern University, Evanston, Illinois*

****Sandia National Laboratories, Albuquerque, New Mexico*

Motivation:

Ordering and pattern formation on surfaces has emerged as a promising way of obtaining new materials with interesting and potentially useful properties. In particular, entirely new self-organized surface alloy phases have recently been created in the laboratory. Understanding why these new phases form, how they form, and how their behavior can be controlled is the main long-term goal of our work. Our goal is to develop a predictive theory of surface alloy thermodynamics that uses realistic surface-atom interactions obtained from first-principles electronic-structure calculations and configurational entropies obtained from Monte-Carlo simulations.

Accomplishment:

Chemical and elastic (both direct and substrate-mediated) interactions between surface atoms play equally important roles in stabilizing observed alloy structures. This property poses a formidable challenge since it requires a theory of surface alloy energetics that includes both positional and configurational degrees of freedom. We have adapted a theory originally developed for bulk alloys and modified it for the case of surface alloys. The Hamiltonian is given by:

$$H = \frac{1}{2} \sum_{\alpha\beta} \sum_{\mathbf{R}, \mathbf{R}'} u_{\alpha}^{*}(\mathbf{R}) \Phi_{\alpha\beta}(\mathbf{R} - \mathbf{R}') u_{\beta}(\mathbf{R}') + \sum_{\alpha} \sum_{\mathbf{R}, \mathbf{R}'} S(\mathbf{R}) K_{\alpha}(\mathbf{R} - \mathbf{R}') u_{\alpha}(\mathbf{R}') + \frac{1}{2} \sum_{\mathbf{R}, \mathbf{R}'} J(\mathbf{R} - \mathbf{R}') S(\mathbf{R}) S(\mathbf{R}'), \quad (*)$$

where $u_{\alpha}(\mathbf{R})$ are atomic displacements, $S(\mathbf{R})$ are pseudo-spin variables (+1 or -1) representing configurational degrees of freedom, and Φ , K , and J are interaction parameters that are obtained using first-principles calculations. Configurational entropy is incorporated by subjecting the Hamiltonian (*) to standard Metropolis Monte Carlo simulations. We have applied the developed formalism to Co-Ag alloys on Ru(0001) surface and obtained excellent agreement with experimental STM images (see below).

Significance:

We have developed a theory of surface alloy thermodynamics that is based upon first-principles energetics and statistical-mechanical treatment of configurational entropies. This theory has reliable predictive capabilities and can be applied to any ultrathin film surface alloy system, and it will be used in subsequent investigations of ordered pattern formation on surfaces.

Publications:

M. Asta, V. Ozolins, and J. J. Hoyt, “The energetics of surface alloy formation: an embedded-atom-method, second-order-expansion study.” *Modeling and Simulation in Materials Science and Engineering* **8**, 287 (2000).

V. Ozolins, M. Asta, and J. J. Hoyt, “Microscopic theory of effective interatomic interactions in surface alloys.” In preparation (2001).

First-Principles Atomistic Model for $\text{Co}_{0.60}\text{Ag}_{0.40}$ on Ru(0001)

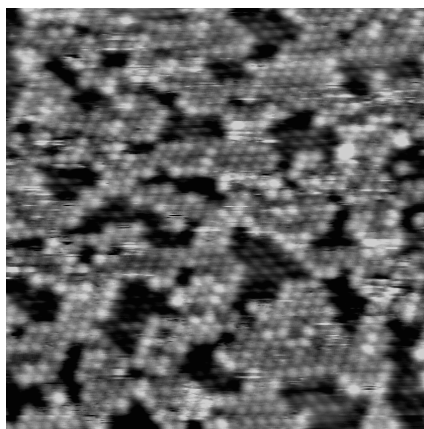


Fig. 1(a)

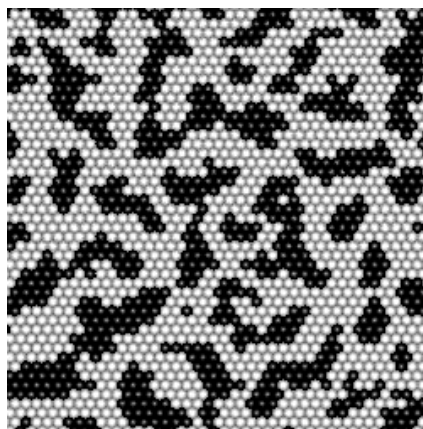


Fig. 1(b)

Figure 1(a) shows an atomic resolution STM image of a 60 at. % Co – 40 at. % Ag monolayer film on Ru(0001), exhibiting a disordered pattern of Ag islands (dark dots) in a Co matrix (gray dots). The sample was annealed at approximately 900 K [see G. Thayer, V. Ozolins, A. K. Schmid, N. C. Bartelt, M. Asta, J. J. Hoyt, S. Chiang, and R. Q. Hwang, “The role of stress in thin-film alloy thermodynamics: Competition between alloying and dislocation formation.”

Physical Review Letters **86**, 660 (2001)]. Figure 1(b) shows a snapshot from Monte Carlo simulations performed at $T=900$ K. Surface atom interactions were calculated theoretically using first-principles electronic-structure methods without any adjustable parameters. The disordered pattern of Ag droplets exhibits the same essential features as the experimental image to the left. Our calculations predict that below ~ 350 K the pattern orders into a regular array of Ag droplets or stripes, depending upon the composition of the surface alloy.

Ab Initio Molecular Dynamics Simulations of Liquid Ni-Al Alloys

M. Asta,* J. J. Hoyt,** V. Ozolins*** and M. van Schilfgaarde***

*Department of Materials Science and Engineering, Northwestern University, Evanston, Illinois

**Sandia National Laboratories, Albuquerque, New Mexico

***Sandia National Laboratories, Livermore, California

Motivation:

Liquid Ni-Al alloys feature significant chemical short-range order, a large mismatch in atomic size, and highly non-ideal thermodynamic solution properties. These melts therefore share many features in common with structurally complex multicomponent liquids used in the processing of commercial alloys and in the production of bulk metallic glasses. The structural and thermodynamic properties of Ni-Al melts have been relatively well characterized, and this binary alloy serves as a non-trivial system for testing the accuracy of various simulation methods. To further understand the microscopic factors influencing non-ideal thermodynamic properties and interatomic diffusion in these alloys, we have for the first time undertaken *ab initio* molecular dynamics (AIMD) simulations of liquid Ni-Al.

Accomplishment:

In Fig. 1 we compare the calculated (solid line) and measured (symbols) Bhatia-Thornton structure factors for a $\text{Ni}_{20}\text{Al}_{80}$ liquid. The agreement between experiment and theory displayed in Fig. 1 is seen to be excellent for both the number-number and number-chemical correlation functions, $S_{NN}(q)$ and $S_{NC}(q)$. The AIMD simulations also reproduce the pronounced peak in the chemical-chemical structure factor (S_{CC}), indicative of a significant chemical short-range order (SRO) in the liquid. The chemical short-range order parameter α_{NiAl} was calculated to be -0.10 , which compares very well with the value of $\alpha_{\text{NiAl}} = -0.09$ derived from neutron-scattering measurements by Maret et al. [Phys. Rev. B **42**, 1598 (1990)]. The average length of Ni-Al bonds is found to be considerably shorter than either Ni-Ni or Al-Al bonds, in contrast with simple-minded hard-sphere considerations and indicative of strong chemical binding between atoms of unlike species. Strong interatomic bonding and chemical short-range order are found to affect the diffusion coefficient. AIMD calculated values of diffusion coefficients are much smaller than those obtained from classical EAM potentials, since the latter do not reproduce well the enhanced bonding and chemical SRO effect between unlike atoms. Finally, we have explained the apparent discrepancy between previously calculated values of excess entropy of formation of liquid Ni-Al alloys and experimental data. It has been attributed to entropy contributions associated with electronic excitations, which were not accounted for in any of the previous classical calculations. The magnitude of electronic excess entropy is calculated to be $\Delta S_{\text{el}} = -0.42 k_B/\text{atom}$, which is 60% of the magnitude of ideal entropy of mixing at the same composition.

Significance:

Using *ab initio* molecular dynamics (AIMD), we were able to reproduce experimentally measured structural and thermodynamic data for liquid Ni-Al alloys. Compared with previous results obtained by classical EAM simulations, AIMD gives rise to a more highly ordered liquid structure leading to lower calculated values for the diffusion coefficients. The AIMD simulations point to a significant non-configurational contribution to the excess entropy of formation for liquid Ni-Al alloys arising from electronic excitations. This contribution is very large ($\Delta S_{\text{el}} = -0.42 k_B/\text{atom}$) and explains previous disagreement between experimental data and classical EAM simulations.

Publication:

M. Asta, J. J. Hoyt, V. Ozolins, and M. van Schilfgaarde, “Ab Initio molecular dynamics study of liquid Ni-Al Alloys.” In preparation (2001).

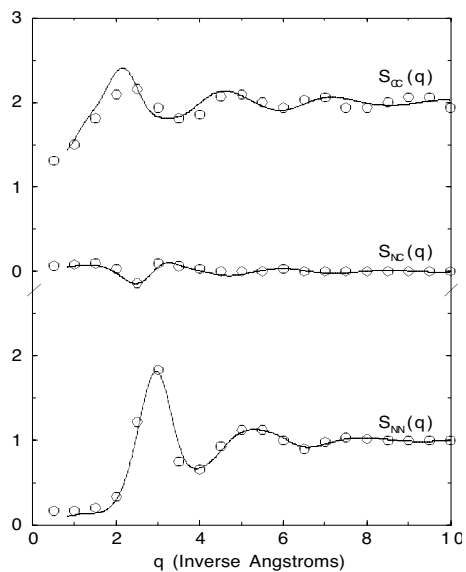


Fig. 1

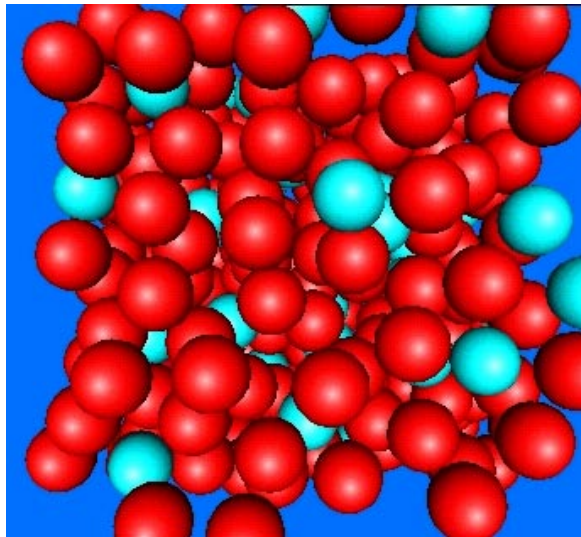


Fig. 2

Figure 1 shows the calculated (solid line) and measured (open symbols) Bhatia-Thornton structure factors for a $\text{Ni}_{20}\text{Al}_{80}$. Figure 2 shows a snapshot of atomic configuration of liquid $\text{Ni}_{0.20}\text{Al}_{0.80}$ at $T=1300$ K. It is apparent from this image that a significant degree of short-range order persists in the liquid, since almost all Ni atoms (cyan) are surrounded by nearest-neighbor Al atoms (red).

Thermodynamic Properties of Al-Cu Alloys

C. Wolverton,* X.-Y. Yan,** R. Vijayaraghavan,* and V. Ozolins

*Ford Motor Company, MD3028/SRL, Dearborn, Michigan

**Dept. of Materials Science and Engineering, Univ. of Wisconsin,
Madison, Wisconsin

***Sandia National Laboratories, Livermore, California

Motivation:

Computational thermodynamic approaches have become a valuable tool in the calculation of complex, multicomponent phase equilibria often found in industrial alloys. These methods rely on databases of free energies, obtained from an optimization process involving experimental thermodynamic and phase diagram data. However, many phases of practical interest (e.g., metastable precipitate phases) are absent from computational thermodynamics databases, due to insufficient information to perform the optimization process. We demonstrate that first-principles, density functional calculations provide a means to obtain thermodynamic functions of phases absent from current databases. As an example to illustrate this hybrid first-principles/computational-thermodynamics approach, we consider the famous metastable Cu-containing precipitate phase, $\text{Al}_2\text{Cu}-\theta'$, often found in age-hardened aluminum alloys.

Accomplishment:

Many classes of industrial aluminum alloys are heat treated in practice to produce increased hardness due to precipitation microstructures. Cu is a commonly occurring solute element which can impart substantial hardening via the precipitates forming along the famous sequence of phase transformations in Al-Cu:

Solid solution \rightarrow GP1, GP2 zones \rightarrow $\text{Al}_2\text{Cu}(\theta')$ \rightarrow $\text{Al}_2\text{Cu}(\theta)$.

The metastable $\text{Al}_2\text{Cu}-\theta'$ phase is an important precipitate in this sequence and can lead to enhanced mechanical properties, but it is unfortunately absent from many computational thermodynamics databases. The reason for this absence is that the thermodynamics of this phase are not well characterized experimentally. In fact, even in the binary Al-Cu system the metastable θ' solvus is not well established.

The phase stability of Al_2Cu in the equilibrium θ and metastable θ' structures has been investigated using first-principles calculations. The surprising result from our work is that *the energetic ground state of Al_2Cu is not θ* , as might be expected from the generally accepted phase diagram. Instead, the calculated $T=0$ energy of the θ' phase is lower than that of θ . This apparent discrepancy between calculated $T=0$ energetics and the experimental observations at finite temperature can be reconciled by appealing to the vibrational entropies of θ and θ' . A significant difference in vibrational entropies between the two phases serves to reverse the $T=0$ energetic tendency and stabilize θ at modest temperatures (i.e., above about 200 C). However, θ' is actually the stable ground state at low temperatures. From these first-principles calculations, one has the energetic and entropic contributions to the stability of θ vs. θ' . Combination of these contributions yields the free energy difference between θ and θ' : $\delta G(\theta'/\theta) = G(\theta') - G(\theta)$. We have used this quantity $\delta G(\theta'/\theta)$ in conjunction with available computational thermodynamics databases to calculate phase diagrams of binary and multicomponent Al-Cu alloys (see Fig. 1 below).

Significance:

Using first-principles methods, we have calculated free energies of θ and θ' phases of Al_2Cu . We have found that the $T=0$ ground state of Al_2Cu is θ' and not θ , as was thought before. We have also shown how to use the calculated first-principles free energy differences to supplement thermodynamic data and construct alloy phase diagrams.

Publications:

C. Wolverton and V. Ozolins, "Entropically favored ordering: The metallurgy of Al_2Cu revisited." Submitted to *Physical Review Letters* (2001).

C. Wolverton, X.-Y. Yan, R. Vijayaraghavan, and V. Ozolins, "Incorporating first-principles free energetics in computational thermodynamics approaches." Submitted to *Acta Materialia* (2001).

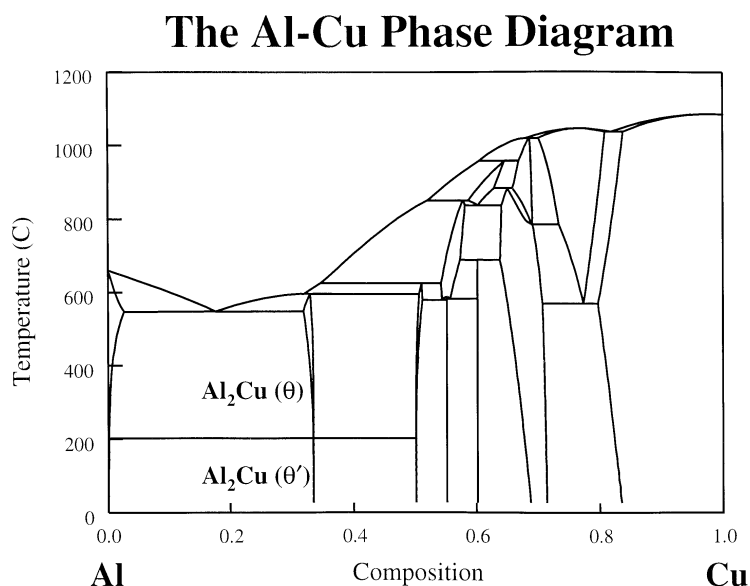


Fig. 1

Fig. 1 shows the equilibrium phase diagram of Al-Cu calculated using the WinPhaD program and database, combined with the first-principles calculated $\delta G(\theta'/\theta)$. As explained above, the first-principles results predict a surprising transition between the stability of θ and θ' around 200 C, and this transition is reflected in Fig. 1.

Thermodynamic Properties of Al-Sc Alloys

V. Ozolins* and M. Asta**

*Sandia National Laboratories, Livermore, California

**Department of Materials Science and Engineering, Northwestern University, Evanston, Illinois

Motivation:

Despite the growing interest in Al(Sc) alloys, uncertainties persist related to the Al-Sc phase diagram. For example, the crystal structure of the equiatomic AlSc phase remains uncertain, with both $B2$ (CsCl prototype) and B_f (BCr prototype) structures having been reported in the literature. Recently, two assessments of the Al-Sc phase diagram have been published by Murray and Cacciamani *et al.* The optimized thermodynamic parameters obtained in these two assessments show significant differences, as do the calculated phase boundaries for near-equiatomic alloy compositions. At present, ternary additions to Al-Sc alloys are being investigated in the development of high specific-strength materials for potential applications at high homologous temperatures. As a basis for modeling phase stability in these multicomponent systems, an improved understanding of the binary Al-Sc phase diagram is desirable.

Accomplishment:

We performed a theoretical study of temperature-dependent structural and thermodynamic properties of solid-phase Al-Sc alloys and compounds based upon first-principles calculations of electronic free energies and ionic vibrational spectra. A large effect of vibrational free energy upon calculated Sc solid solubility limits is found. The contributions of non-configurational (electronic and vibrational) entropies to the free energies of solid-phase Al-Sc alloys and compounds are analyzed, and the accuracy of the approximations employed in these calculations is assessed. For each of the reported intermetallic compounds in this system, calculated formation enthalpies agree to within ten percent (0.05 eV/atom) of published calorimetric measurements. Large negative entropies of formation, equal to -0.77, -0.28 and -0.62 k_B /atom are calculated for cubic Al_3Sc , cubic AlSc and orthorhombic AlSc compounds, respectively, resulting primarily from the stiffening of nearest-neighbor Al-Sc bonds in the intermetallic phases relative to elemental Al and Sc. The net effects of non-configurational free energy contributions to the fcc portion of the Al-Sc phase diagram are 100 and 450 K decreases in calculated Al solvus phase boundary temperatures associated with electronic and vibrational entropy, respectively, at the maximum measured Sc solid-solubility limit. It is suggested that vibrational entropy may stabilize the orthorhombic B_f phase of AlSc just below the melting temperature.

Significance:

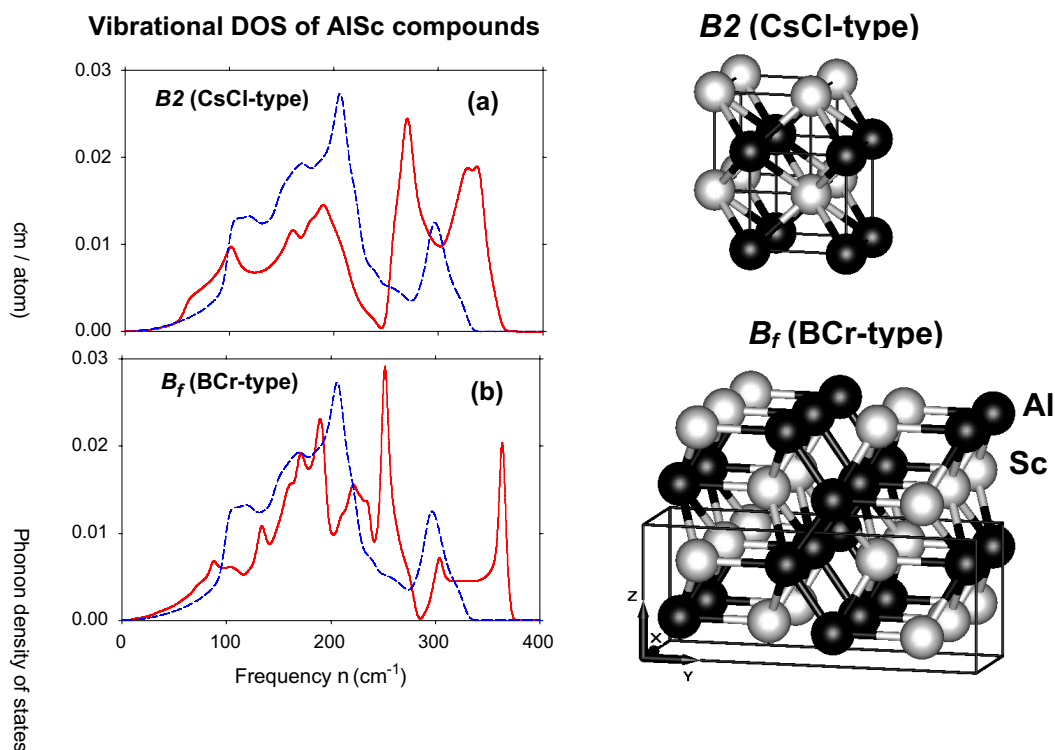
Our results point to a substantial effect of vibrational entropy upon calculated temperatures for phase boundaries between substitutional alloy phases with differing compositions. Further work on other Al-based alloy systems is currently being performed to assess the generality of our findings for Al-rich Al-Sc alloys. Preliminary results and previous analysis by Zener [*Thermodynamics in Physical Metallurgy*, edited by C. Zener (ASM, Cleveland OH, 1950), pp. 16-27] suggest that vibrational entropy leads to significant reductions in the temperature scales of calculated phase boundaries in a wide range of Al-based

alloys. Vibrational entropy may also tend to stabilize low-symmetry phases, such as orthorhombic B_f vs. cubic $B2$ in AlSc.

Publications:

V. Ozolins and M. Asta, "Large vibrational effects upon calculated phase boundaries in Al-Sc." *Physical Review Letters* **86**, 448 (2001).

M. Asta and V. Ozolins, "Structural, vibrational and thermodynamic properties of Al-Sc alloys and intermetallic compounds." Submitted to *Physical Review B* (2001).



Calculated phonon DOS of ordered AlSc compounds (red lines, left panel). Blue dashed line shows the composition-weighted phonon DOS of constituents. Due to less weight in the low-frequency region, both compounds exhibit negative entropies of formation. Crystal structure of the cubic $B2$ and orthorhombic B_f structures are shown to the right. The orthorhombic B_f structure has a higher vibrational entropy and is predicted to be stable just below the melting point of AlSc.

Imaging the Oxidation of the NiAl (110) Surface

K. F. McCarty

Sandia National Laboratories, Livermore, CA 94551

Motivation:

One method of making metal/ceramic interfaces is by oxidizing a metal alloy. In particular, a procedure to make thin, uniform films of crystalline alumina has been developed based upon oxidizing the (110) surface of the ordered intermetallic alloy NiAl. Here we use real-time microscopy to reveal how the oxide nucleates and grows.

Accomplishment:

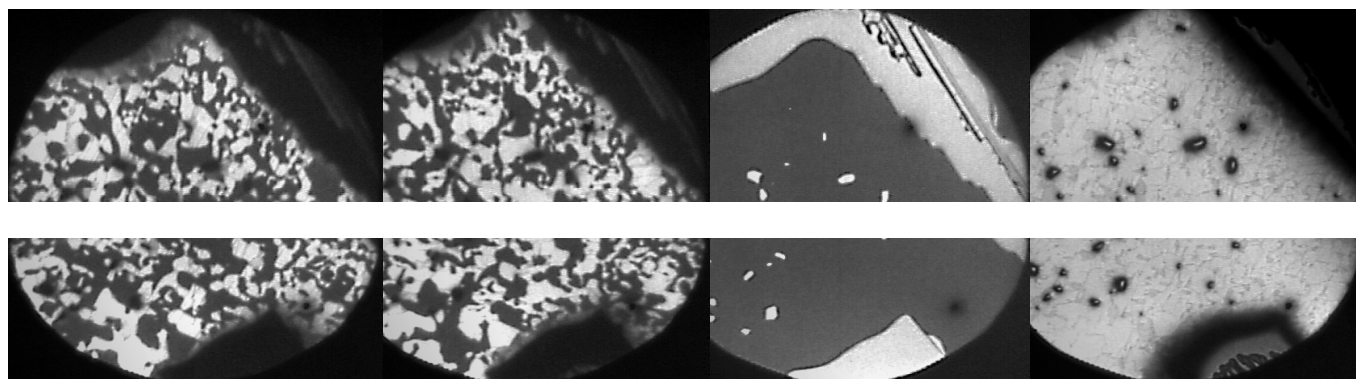
We have used low-energy electron microscopy (LEEM) to selectively image the different surface phases that form as the NiAl (110) surface undergoes oxidation. The clean surface was exposed to O₂ at 325°C and then imaged at progressively higher temperatures. While a relatively uniform film results, oxide-free regions (pinholes) develop when the initially amorphous oxide crystallizes. This oxide film consists of one type of alumina that has two orientational domains on the substrate. Selective imaging of the domains just after crystallization shows that nuclei of both domains are present at high density. With time and temperature, the domains coarsen greatly, as do the oxide-free regions (pinholes). (See Figure.) By reducing the length of the domain boundaries, the coarsening reduces the energy.

Significance:

Metal/oxide interfaces are important for ceramic joining, electrical interconnects in microelectronics, supported catalysts, and chemical sensors. For the first time, we have shown that phase-specific imaging of an alloy's surface can be performed in real time as a metal/ceramic interface forms. We directly observe how nucleation and growth occurs and find, unexpectedly, that pinholes develop when the oxide crystallizes.

Reference:

K. F. McCarty,, "Imaging the Crystallization and Growth of Oxide Domains on the NiAl (110) Surface," Surface Science, in press (2001).



i) DF-Ox1

ii) DF-Ox2

iii) DF-NiAl

iv) BF

Figure. LEEM images obtained at 1015°C (5 μm field of view). In images i) and ii), the bright regions correspond selectively to one of the two oxide domains. However, the bright areas in image iii) are regions of bare substrate, showing that the surface is not completely covered with oxide. In the bright-field image (iv), these regions of unoxidized NiAl substrate appear as dark spots.

Bulk Vacancies are Created at Surface Steps

K. F. McCarty, J. A. Nobel, and N. C. Bartelt
Sandia National Laboratories, Livermore, CA 94551

Motivation:

Since thermally generated vacancies in solids are known to control many materials properties (e.g., solid-state diffusion), it is important to understand how thermal vacancies are created and destroyed. Where and how vacancies on surfaces are generated has not been directly established. For example, it is unknown whether bulk vacancies are created over the entire area of a surface, or only at selected sites, such as surface steps.

Accomplishment:

We have used low-energy-electron microscopy (LEEM) to study in real time vacancy generation on the (110) surface of the ordered intermetallic alloy NiAl. We oscillate the sample's temperature and observe the response of the nanoscale surface structure as a function of frequency (a version of Ångström's method of measuring thermal conductivity). We find that vacancies are generated (and annihilated) not over the entire surface, but only near atomic step edges (see Figure).

Significance:

To our knowledge, this is the first direct demonstration of where bulk vacancies are formed at a surface. That vacancies on the NiAl (110) surface are generated and annihilated only near the step edges undoubtedly affects how other processes involving vacancies (e.g., surface oxidation) actually occur. We have also demonstrated a new and powerful way to measure important properties of bulk materials. We use the technique to explicitly determine the migration and formation energies of the bulk defects in NiAl, the prototypical high-temperature alloy. More importantly, we demonstrate that our technique can be used to unambiguously determine the thermal-defect type as a function of temperature and composition.

Reference:

K. F. McCarty, J. A. Nobel, and N. C. Bartelt, "Vacancies in solids and the stability of surface morphology," submitted (2001).

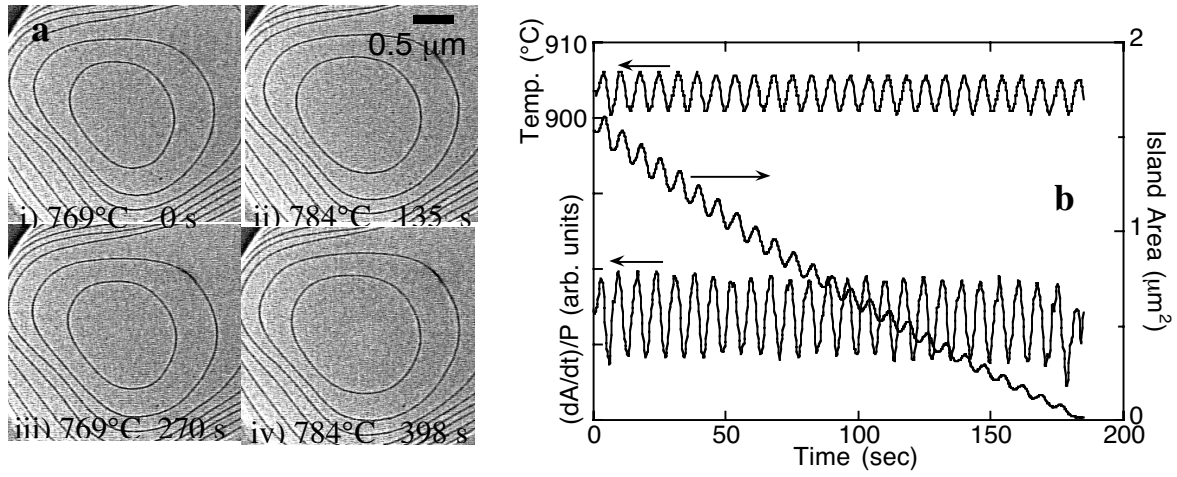


Figure a) LEEM micrographs of an island-stack structure on the NiAl (110) surface as the temperature is varied about a mean of 776°C. With increasing temperature, bulk atoms come to surface since the concentration of thermal vacancies in the bulk increases. For decreasing temperature, the islands shrink in size because material leaves the surface to reduce the bulk vacancy concentration.

b) Island area $A(t)$ and the rate of change normalized by the perimeter $(dA/dt)/P$ as the temperature is a sinusoidally oscillated by about $\pm 2.5^\circ\text{C}$ around a mean of 903°C. Even though the island area decreases greatly because of thermal smoothing, the area change resulting from the temperature oscillation scales exactly as the perimeter of the island.